Reproducibility and Replicability in Neuroimaging: Constrained IVA as an Effective Assessment Tool

Francisco Laport[1,2], Adriana Dapena[2], Trung Vu[1], Hanlu Yang[1], Vince Calhoun[3] and Tülay Adali[1]
[1]Department of Computer Science and Electrical Engineering, University of Maryland Baltimore County, MD, 21250, USA
[2]CITIC Research Center, University of A Coruña, 15071 A Coruña, Spain
[3]Tri-Institutional Center for Translational Research in Neuroimaging and Data Science (TReNDS),
Georgia State University, Georgia Institute of Technology, and Emory University, Atlanta, GA 30303, USA
Email: [1]{flopez2, trungvv, hyang3, adali}@umbc.edu, [2]{francisco.laport, adriana.dapena}@udc.es, [3]vcalhoun@gsu.edu

***Abstract*—Matrix decomposition techniques have been successfully applied in the analysis of multi-subject functional magnetic resonance imaging (fMRI) data. These data-driven approaches that assume the linear blind source separation (BSS) problem can yield an unsupervised and fully interpretable solution when there is a good model match. However, selecting a suitable model order that provides an accurate model match is an important challenge. Replicability and computational reproducibility are two key aspects that are also intimately related to interpretability. Despite clear evidence that solutions with poor reproducibility can lead to suboptimal results, the evaluation of reproducibility in matrix decomposition techniques remains limited in the existing literature. We propose the use of constrained independent vector analysis (cIVA), a state-of-the-art joint BSS technique, to assess the influence of model order selection for replicability and reproducibility. We demonstrate the attractiveness of cIVA for replicability by alleviating permutation ambiguity as well as enabling additional quantification opportunities. Our results show that highly reproducible model orders achieve a good model match with highly interpretable and replicable solutions when cIVA is applied to four different resting-state fMRI datasets.**

***Index Terms*—independent vector analysis, reproducibility, replicability, fMRI analysis.**

I. Introduction

Data-driven approaches have been playing an important role in the analysis of large-scale multi-subject functional magnetic resonance imaging (fMRI) data, allowing us to study brain functional connectivity and the subsequent identification of biomarkers for different brain disorders such as schizophrenia or bipolar disorder [1], [2]. However, unlike model-based approaches, data-driven solutions often lack a clear connection to a physical model. Therefore, an emphasis is placed on the interpretability of the results [3]. Matrix decomposition techniques, due to their connection with the linear blind source separation (BSS) problem, provide an unsupervised solution that is fully interpretable. In this regard, independent component analysis (ICA), a popular BSS technique, assumes a linear combination of latent variables in the observed data and implements a matrix decomposition approach to extract the variables of interest, where the rows/columns of the estimated factors can be associated with (physical) quantities of interest [3]. In fMRI data, the rows/columns of the decomposed matrices can be related to spatially independent functional networks and their corresponding time courses [1], [4].

Reproducibility and replicability are two important considerations that are closely tied to a good interpretation of the results. According to the US National Academies of Sciences, Engineering, and Medicine [5], (computational) reproducibility is defined as obtaining consistent results using the same data and code. On the other hand, replicability is defined as obtaining consistent results using the same code but different data. Hence, if the results are not consistent and generalizable, they will be hardly interpretable and of limited value.

When multi-subjects datasets are available, joint BSS (JBSS) can be applied to obtain more effective decompositions by exploiting the joint information across subjects [6]. Independent vector analysis (IVA) is a JBSS technique that extends ICA by leveraging statistical dependencies across multiple datasets through a multivariate density model to achieve a powerful and fully interpretable decomposition [4], [6], [7]. IVA has proved to be an effective technique for preserving inter-subject variability in the fMRI analysis [8]. Also, IVA presents uniqueness guarantees under general conditions, which is an important property to ensure interpretability [4]. However, IVA is computationally expensive and its performance degrades as the number of datasets increases [9]. To mitigate these drawbacks, constrained IVA (cIVA) was proposed, which incorporates prior information to the analysis to improve IVA performance in large-scale multi-subject datasets while preserving the interpretability properties of IVA [9]. Additionally, cIVA alleviates the permutation ambiguity of IVA by aligning the components and their estimations, which facilitates the post-analysis of the results and allows us to effectively conduct a replicability study across datasets [10].

Even though JBSS techniques have been successfully applied in neuroimaging analysis, the evaluation of their computational reproducibility has been limited [3], [11]. Considering that the cost functions of most JBSS algorithms are non-convex, convergence can only be guaranteed to a local optimum. Moreover, iterative methods, usually with random initializations, are often implemented since closed-form solutions do not exist for these problems [3], [11], [12]. Hence, even

This work is supported in part by the grants NSF 2316420, NIH R01MH118695, NIH R01MH123610, NIH R01AG073949, Xunta de Galicia (grants ED431C 2020/15 and ED481B 2022/012), MCIN/AEI/10.13039/501100011033 and by the European Union NextGenerationEU/PRTR (grant TED2021-130240B-I00 (IVRY))

though all the algorithmic quantities are fixed, the obtained results can be quite different due to the variability introduced by the initialization. Therefore, to evaluate reproducibility, a suitable metric must be selected to measure the consistency of the results. Most reproducible solutions have been shown to lead to results with better interpretability [3], [11].

Due to the bias and variance dilemma in estimation theory, a reproducible solution with low variability might not have enough flexibility to capture the important features of the data and yield a high bias, and vice versa. In this regard, cIVA introduces reliable prior information to the model which guides the algorithms to avoid a suboptimal solution, hence, achieving a good balance between bias and variance even when used in conjunction with a flexible approach. Furthermore, the model order and its complexity significantly influence the quality and consistency of the results. The proper selection of the model order is an important challenge that plays a key role in model match, and an accurate model match that properly represents the features of the observed data, enhances the reproducibility and interpretability of the estimates [3].

In this work, we assess the replicability and computational reproducibility of cIVA as a function of the model order. We show that those model orders that offer the most consistent results lead to better quality estimates and more interpretable and replicable functional networks. Moreover, we also demonstrate the effectiveness of cIVA to conduct a replicability study, providing additional quantification opportunities when applied to four different resting-state fMRI datasets. The rest of this paper is organized as follows. Section II describes the employed methods. Section III presents the obtained results by the cIVA algorithm, and Section IV explains the main conclusions of this study.

II. Methodology

A. Independent Vector Analysis (IVA)

Consider K datasets $\boldsymbol{x}^{[k]}(v) \in \mathbb{R}^N$ composed by V samples ($v = 1 \dots V$) and where each dataset $\boldsymbol{x}^{[k]}(v) = [\boldsymbol{x}_1^{[k]}(v), \dots, \boldsymbol{x}_N^{[k]}(v)] \in \mathbb{R}^N$ is modeled as a linear mixture of N latent sources $\boldsymbol{s}^{[k]}(v) = [\boldsymbol{s}_1^{[k]}(v), \dots, \boldsymbol{s}_N^{[k]}(v)] \in \mathbb{R}^N, 1 \leq k \leq K$. Then, the IVA generative model is defined as

$$\boldsymbol{x}^{[k]}(v) = \boldsymbol{A}^{[k]}\boldsymbol{s}^{[k]}(v), \tag{1}$$

where $\boldsymbol{A}^{[k]} \in \mathbb{R}^{N\times N}$ is an invertible mixing matrix. IVA estimates K demixing matrices $\boldsymbol{W}^{[k]} \in \mathbb{R}^{N\times N}$ to compute the source estimates $\boldsymbol{y}^{[k]}(v) = [\boldsymbol{y}_1^{[k]}(v), \dots, \boldsymbol{y}_N^{[k]}(v)] \in \mathbb{R}^N$, where $\boldsymbol{y}^{[k]}(v) = \boldsymbol{W}^{[k]}\boldsymbol{x}^{[k]}(v)$.

By stacking the nth latent source across the K datasets, we define a source component vector (SCV) $\boldsymbol{s}_n(v) = [s_n^{[1]}(v), \dots, s_n^{[K]}(v)]^\top$. Hence, we also define $\boldsymbol{y}_n(v) = [y_n^{[1]}(v), \dots, y_n^{[K]}(v)]^\top \in \mathbb{R}^K$ as the nth estimated SCV. Assuming the latent SCVs are independent, the goal of IVA is to maximize the independence between the N SCVs by minimizing the mutual information among the estimated SCVs. To this end, to exploit the statistical dependencies across datasets, IVA models each SCV with a multidimensional probability density function (PDF). The IVA cost function is given as [4], [6]

$$\mathcal{J}_{\text{IVA}}(\mathcal{W}) = \sum_{n=1}^{N}\left(\sum_{k=1}^{K}\mathcal{H}(\boldsymbol{y}_n^{[k]}) - \mathcal{I}(\boldsymbol{y}_n)\right) - \sum_{k=1}^{K}\log\left|\det(\boldsymbol{W}^{[k]})\right|,$$

where $\mathcal{W} = \{\boldsymbol{W}^{[k]}\}_{k=1}^{K}$, $\mathcal{H}(\boldsymbol{y}_n^{[k]})$ denotes the entropy of the nth source estimate for the kth dataset and $\mathcal{I}(\boldsymbol{y}_n)$ denotes the mutual information of the nth SCV. We can see that the cost function simultaneously maximizes the independence within a dataset with the entropy term and also maximizes the dependence across datasets by maximizing the dependence among components within each SCV.

Multivariate Gaussian distribution (MGD) is an attractive solution for modeling the SCVs. In this case, the IVA algorithm (IVA-G) [6], [13], only exploits second-order statistics by minimizing the correlation between SCVs and maximizing the correlation within each SCV. Multivariate Laplacian distributions have been shown to provide a better model match with latent fMRI sources [9]. However, it is a computationally expensive approach. Using cIVA we incorporate reference signals into the IVA-G analysis to guide the decomposition, limit the solution space, and maintain the model match while providing a computationally efficient estimation [10], [14].

B. Constrained IVA

Consider a set of references $\{\boldsymbol{r}_n\}_{n=1}^{M} \subset \mathbb{R}^V (M \leq N)$, the main goal is to maximize the similarity between $\boldsymbol{r}_n$ and the corresponding estimated SCV $\boldsymbol{y}_n$ while also minimizing similarity with the other estimated SCV $\boldsymbol{y}_m$ where $n \neq m$. For this purpose, we employ the regularization as in [10]

$$\mathcal{J}_{\text{ref}}(\mathcal{W}) = \sum_{n=1}^{M}\sum_{k=1}^{K}\left(\sum_{\substack{m=1\\ m\neq n}}^{M}\epsilon^2(\boldsymbol{r}_n, \boldsymbol{y}_m^{[k]}) - \epsilon^2(\boldsymbol{r}_n, \boldsymbol{y}_n^{[k]})\right), \tag{2}$$

where $\epsilon : \mathbb{R}^V \times \mathbb{R}^V \to [0, 1]$ is implemented as the absolute value of the Pearson correlation. The augmented cost function is a linear combination of the IVA-G cost function and the regularization term

$$\mathcal{L}_\lambda(\mathcal{W}) = \mathcal{J}_{\text{IVA-G}}(\mathcal{W}) + \frac{\lambda}{2}\mathcal{J}_{\text{ref}}(\mathcal{W}), \tag{3}$$

where the regularization parameter λ balances the impact of the IVA-G cost $\mathcal{J}_{\text{IVA-G}}$ and the regularization term. After studying different λ values, we decided to set $\lambda = 100$ as the value that provides more interpretable results. Thanks to the regularization term, cIVA alleviates the permutation ambiguity inherent in matrix decompositions and enhances replicability when applied to different datasets, as each constrained source is automatically aligned to its corresponding reference.

C. Cross-joint-ISI

Joint intersymbol interference (joint-ISI) [6] is a popular metric to evaluate JBSS techniques when the ground truth mixing matrices $\boldsymbol{A}^{[k]}$ are available. This is an extension of the normalized ISI to the case of multiple datasets. Let

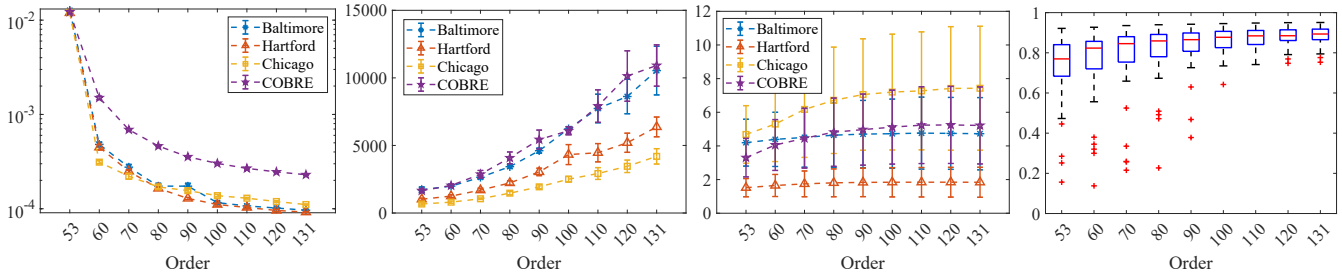

(a) Partial cross-joint-ISI (b) Runtime (seconds) (c) Power ratio (d) Mean component correlation

Fig. 1: Comparison of different model orders for four real fMRI datasets. Only the 53 RSNs related to the references are analyzed. The partial cross-joint-ISI (a) and runtime (b) are shown for 50 independent runs. Plot (c) shows the power ratio for the most reproducible run and plot (d) shows the correlation of the mean component (across subjects) among the four datasets.

$\boldsymbol{G}^{[k]} = \boldsymbol{A}^{[k]}\boldsymbol{W}^{[k]}$, for $k = 1, \ldots, K$, be the global mixing-demixing matrices and $\boldsymbol{G} = 1/K \sum_{k=1}^{K} |\boldsymbol{G}^{[k]}|$ be their mean absolute matrix. The joint-ISI of $\boldsymbol{G}^{[1]}, \ldots, \boldsymbol{G}^{[K]}$ is defined as the ISI of $\boldsymbol{G}$, where

$$\text{ISI}(\boldsymbol{G}) = \frac{\sum_{i=1}^{N}\left(\frac{\sum_{j=1}^{N}|G_{ij}|}{\max_p |G_{ip}|} - 1\right) + \sum_{j=1}^{N}\left(\frac{\sum_{i=1}^{N}|G_{ij}|}{\max_p |G_{pj}|} - 1\right)}{2N(N-1)},$$

where G_{ij} is the (i, j)-entry of $\boldsymbol{G}$. In the case of perfect source separation, $\boldsymbol{G}$ is an identity matrix subject to permutation and scaling ambiguities, thus achieving zero joint-ISI.

In practical problems where the ground truth is unknown, cross-joint-ISI is proposed to measure the consistency of the estimated components across R runs. It is defined as cross-joint-ISI$_{ij}(\{\boldsymbol{W}_r^{[k]}\}_{r=1,k=1}^{R,K})$ = joint-ISI$(\boldsymbol{P}_{i,j}^{[1]}, \ldots, \boldsymbol{P}_{i,j}^{[K]})$, where $\boldsymbol{P}_{i,j}^{[k]} = \boldsymbol{A}_i^{[k]}\boldsymbol{W}_j^{[k]}$, $\boldsymbol{A}_i^{[k]} = (\boldsymbol{W}_i^{[k]})^{-1}$ is the inverse of the kth demixing matrix of the ith run, and $\boldsymbol{W}_j^{[k]}$ is the kth demixing matrix of the jth run. The cross-joint-ISI of the ith run is computed by averaging all its pairwise cross-joint-ISI values:

$$\text{cross-joint-ISI}_i = \frac{1}{R}\sum_{j=1, j\neq i}^{R} \text{cross-joint-ISI}_{ij}. \quad (4)$$

Values closer to zero will indicate a higher consistency and reproducibility of the results. Note that by taking the M rows/columns of $\boldsymbol{W}^{[k]}$ and $\boldsymbol{A}^{[k]}$, respectively, this method can be partially computed for those M constrained components, which we refer as partial cross-joint-ISI in the rest of the paper.

III. Experimental Results

A. Resting-State fMRI Data

This study analyzes resting-state fMRI data from four different datasets. Three of them are part of the bipolar-schizophrenia network on intermediate phenotypes (B-SNIP) study [15], and the fourth dataset was collected by the Center of Biomedical Research Excellence (COBRE) [16]. For B-SNIP, data from healthy controls (HC) and schizophrenia patients (SZ) in Baltimore, Hartford, and Chicago were employed. An open-eyes 5-minute run was captured for each subject. The fMRI data were captured by a 3-Tesla Siemens Triotim scanner with TE = 30 ms and voxel size = $3.4 \times 3.4 \times 3$ mm^3. For Baltimore, 134 time points were captured with TR = 2.21 s, while 201 time points were obtained in Hartford and Chicago with TR = 1.5 s and TR = 1.775 s, respectively. We removed the first 3 time points to address the T-1 effect and data was preprocessed including motion and slice-time correction. Data were resampled to $3 \times 3 \times 3$ mm^3 isotropic voxels. Each subject image was masked, yielding an observation vector of $V = 50223$ voxels for each time point.

In the case of COBRE, an open-eyes 5-minute scan consisting of 150 time points was obtained for each subject. The fMRI data were captured in a 3-Tesla Siemens Trio scanner with TE = 29 ms, TR = 2 s, and voxel size = $3.4 \times 3.4 \times 3$ mm^3. The first 6 time points were removed to address the T-1 effect and each subject's image data was preprocessed including motion and slice-time correction. Data were resampled to $3 \times 3 \times 3$ mm^3 isotropic voxels. Finally, each subject's data were masked obtaining an observation vector of $V = 59255$ voxels for each time point. The subject distribution is as follows: Baltimore 49 HC and 49 SZ; Hartford 38 HC and 38 SZ; Chicago 30 HC and 30 SZ; and COBRE 49 HC and 49 SZ. For each dataset, we wanted to keep a balanced number of subjects in each group to avoid bias in the conducted experiments. Some datasets were composed of fewer subjects, which limited the maximum number in the analysis.

B. Results and Discussion

In this section, we evaluate the reproducibility, replicability, and interpretability of the results obtained by cIVA-G as a function of the model complexity. To this end, the algorithm is applied to four real fMRI datasets using various model orders. Neuromark_fMRI_1.0 functional template [2] is employed as the reference signals. It is composed of 53 resting-state networks (RSNs) from seven different functional domains: sub-cortical (SC, 5 RSNs), auditory (AUD, 2 RSNs), motor (MOT, 9 RSNs), visual (VIS, 9 RSNs), cognitive control (CC, 17 RSNs), default mode (DMN, 7 RSNs) and cerebellar (CB, 4 RSNs). All the RSNs from the templates were used as references ($M = 53$), while the total number of estimated components were in the range $\{53, 131\}$. Notably, when

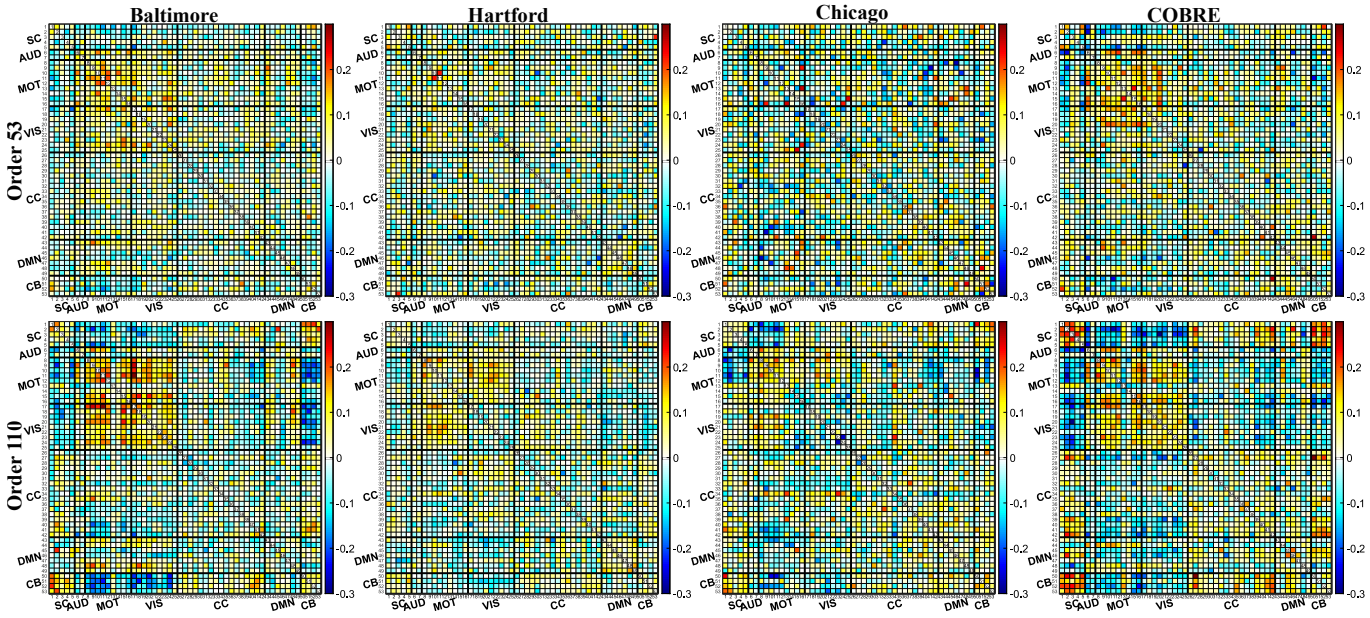

Fig. 2: Difference mean FNC maps (HC-SZ). Pairwise Pearson correlation between estimated RSNs time courses are first Fisher z-transformed and averaged across HC and SZ subjects, respectively. Positive values indicate higher connectivity in HC. Only the 53 RSNs related to the references are analyzed.

$N > M$, the free components capture information due to interference/noise as well as components that might not be in the reference set.

Fifty independent runs with random initializations were performed for each model order and dataset. The partial cross-joint-ISI values for those components associated with a reference signal are presented in Fig. 1-a. As can be appreciated, the model order is closely related to the reproducibility of the results, as the model order increases the partial cross-joint-ISI decreases. This can be explained as fMRI data may include unwanted signals like motion-related artifacts, scanner-related noise, or magnetic resonance acquisition interference. Hence, when the number of estimated components is higher, we can capture the effect of interference and noise as well as components that do not match with the templates thus increasing the overall estimation performance, especially for the networks that match to a functional template. As a consequence, those components related to the references will show lower variability and, therefore, more reproducible results. It is important to note that this improvement in reproducibility is tied to higher model complexity and a larger computational cost, as can be observed in Fig. 1-b.

In fMRI data, low-frequency activity is typically linked to BOLD (Blood Oxygen Level Dependent) signals, so a good metric to assess the interpretability of the results is to analyze the power spectra of the RSN time courses (columns of $\boldsymbol{A}^{[k]}$) and the power ratio between low-frequency (< 0.1 Hz) and high-frequency (> 0.15 Hz) bands. A higher power ratio will indicate brain activity. Conversely, lower power ratios will be related to cardiac or respiratory activity [17]. Fig. 1-c shows the power ratios of the most consistent run for each dataset and model order. We can appreciate that as we increase the order, the power ratio also increases. This improvement is more significant in COBRE and Chicago, but the four datasets show the same trend. We can also see that the mean power ratio becomes more stable for higher orders and that after the order 100 there are no significant improvements. Fig. 1-d analyzes the replicability of the results by showing the correlation of the mean spatial maps between datasets. As observed, larger orders present more replicable solutions, offering more stable results with higher similarities between datasets.

Considering the obtained results, we can appreciate that there is a trade-off between the computational cost and the reproducibility, interpretability, and replicability of the estimates. We consider that order 110 offers a suitable balance in this trade-off, achieving a good model match with reproducible and replicable solutions. Therefore, we further analyze the results obtained by this model order. The functional network connectivity (FNC) map shows the temporal correlation between components. We expect HC to present higher connectivity than SZ patients within each functional domain and also between sensory-related areas such as VIS and MOT. Fig. 2 shows the difference between the mean FNCs for each group (HC-SZ) for the four datasets with orders 53 and 110. We can appreciate higher similarities between FNC maps in the higher order. Also, group differences are more notable and consistent across datasets such as those found within MOT, SC, and CB and between MOT and VIS, VIS and CB, MOT and CB, MOT and SC, or CB and SC, which agree with previous studies [2], [17]. This increases our confidence that a highly reproducible model complexity will also achieve a better model match and, as a consequence, more interpretable and replicable results.

For a more comprehensive analysis, we also assess the replicability of the estimated spatial maps. Fig. 3-a shows

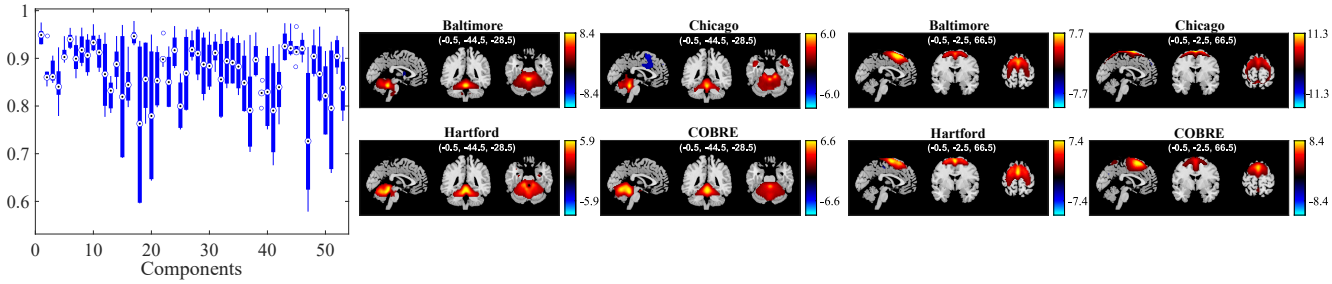

(a) Mean component correlation (b) Cerebellar resting-state network (c) Motor resting-state network

Fig. 3: Mean component correlation and free-components spatial maps for order 110. Plot (a) shows the pairwise correlation between datasets of each estimated component associated with a reference. Notice similar trends for the components. Plots (b) and (c) show the average spatial maps for two estimated free components for the four datasets.

the pairwise correlation of each component between the four datasets. We can see that cIVA-G obtains highly replicable spatial maps, with correlations above 0.57 for all the estimates associated with a reference signal. It is important to highlight that for these components the algorithm achieves interpretable and clear spatial maps, where the correlations between individual subjects' components and the reference signals range from 0.3 to 0.7. We also analyze the spatial maps of the free components. Fig. 3-b and 3-c show two commonly estimated free components in the four datasets. These results suggest that unconstrained IVA-G also achieves a replicable and interpretable estimation and increases our confidence in leaving free components in the analysis.

IV. Conclusions

We analyzed the reproducibility and replicability of a data-driven technique, such as cIVA, as a function of the model order when applied to four different fMRI datasets. We demonstrate that cIVA is a powerful technique that allows us to effectively assess replicability by alleviating the permutation ambiguity as well as providing additional quantification opportunities. The results demonstrated that highly reproducible model orders achieve a better model match with more interpretable functional networks and more replicable solutions. Future work will study the impact of the number of time points and the sample size on the interpretability of the solutions [18]. The FNC maps obtained by the two larger datasets show more robust group differences than those achieved by the two smaller sets. Hence, the sample size and its influence on interpretability is a key aspect to be further analyzed.

References

[1] V. D. Calhoun and T. Adalı, "Multisubject independent component analysis of fMRI: A decade of intrinsic networks, default mode, and neurodiagnostic discovery," *IEEE Trans. Biomed. Eng.*, vol. 5, pp. 60–73, 2012.

[2] Y. Du, Z. Fu, J. Sui, S. Gao, Y. Xing, D. Lin, M. Salman, A. Abrol, M. A. Rahaman, J. Chen *et al.*, "NeuroMark: An automated and adaptive ICA based pipeline to identify reproducible fMRI markers of brain disorders," *NeuroImage Clin.*, vol. 28, p. 102375, 2020.

[3] T. Adali, F. Kantar, M. A. B. S. Akhonda, S. Strother, V. D. Calhoun, and E. Acar, "Reproducibility in matrix and tensor decompositions: focus on model match, interpretability, and uniqueness," *IEEE Signal Process. Mag.*, vol. 39, no. 4, pp. 8–24, 2022.

[4] T. Adalı, M. Anderson, and G.-S. Fu, "Diversity in independent component and vector analyses: Identifiability, algorithms, and applications in medical imaging," *IEEE Signal Process. Mag.*, vol. 31, no. 3, pp. 18–33, 2014.

[5] National Academies of Sciences, Engineering, and Medicine, *Reproducibility and replicability in science*. National Academies Press, 2019.

[6] M. Anderson, T. Adalı, and X.-L. Li, "Joint blind source separation with multivariate Gaussian model: Algorithms and performance analysis," *IEEE Trans. Signal Process.*, vol. 60, no. 4, pp. 1672–1683, 2011.

[7] T. Kim, T. Eltoft, and T.-W. Lee, "Independent vector analysis: An extension of ICA to multivariate components," in *Independent Component Analysis and Blind Signal Separation*. Springer, 2006, pp. 165–172.

[8] E. A. Allen, E. B. Erhardt, Y. Wei, T. Eichele, and V. D. Calhoun, "Capturing inter-subject variability with group independent component analysis of fMRI data: a simulation study," *Neuroimage*, vol. 59, no. 4, pp. 4141–4159, 2012.

[9] S. Bhinge, R. Mowakeaa, V. D. Calhoun, and T. Adalı, "Extraction of time-varying spatiotemporal networks using parameter-tuned constrained IVA," *IEEE Trans. Med. Imag.*, vol. 38, no. 7, pp. 1715–1725, 2019.

[10] T. Vu, F. Laport, H. Yang, V. D. Calhoun, and T. Adali, "Constrained independent vector analysis with reference for multi-subject fMRI analysis," *arXiv preprint arXiv:2311.05049*, 2023.

[11] T. Adali and V. D. Calhoun, "Reproducibility and replicability in neuroimaging data analysis," *Curr. Opin. Neurol.*, vol. 35, no. 4, pp. 475–481, 2022.

[12] Q. Long, C. Jia, Z. Boukouvalas, B. Gabrielson, D. Emge, and T. Adalı, "Consistent run selection for independent component analysis: Application to fMRI analysis," in *Proc. IEEE Int. Conf. Acoust. Speech Signal Process.* IEEE, 2018, pp. 2581–2585.

[13] M. Anderson, G.-S. Fu, R. Phlypo, and T. Adalı, "Independent vector analysis: Identification conditions and performance bounds," *IEEE Trans. Signal Process.*, vol. 62, no. 17, pp. 4399–4410, 2014.

[14] S. Bhinge, Q. Long, Y. Levin-Schwartz, Z. Boukouvalas, V. D. Calhoun, and T. Adalı, "Non-orthogonal constrained independent vector analysis: Application to data fusion," in *Proc. IEEE Int. Conf. Acoust. Speech Signal Process.* IEEE, 2017, pp. 2666–2670.

[15] C. A. Tamminga, E. I. Ivleva, M. S. Keshavan, G. D. Pearlson, B. A. Clementz, B. Witte, D. W. Morris, J. Bishop, G. K. Thaker, and J. A. Sweeney, "Clinical phenotypes of psychosis in the bipolar-schizophrenia network on intermediate phenotypes (B-SNIP)," *Am. J. Psychiatry*, vol. 170, no. 11, pp. 1263–1274, 2013.

[16] A. Scott, W. Courtney, D. Wood, R. De la Garza, S. Lane, M. King, R. Wang, J. Roberts, J. A. Turner, and V. D. Calhoun, "COINS: an innovative informatics and neuroimaging tool suite built for large heterogeneous datasets," *Front. Neuroinform.*, vol. 5, p. 33, 2011.

[17] E. A. Allen, E. B. Erhardt, E. Damaraju, W. Gruner, J. M. Segall, R. F. Silva, M. Havlicek, S. Rachakonda, J. Fries, R. Kalyanam *et al.*, "A baseline for the multivariate comparison of resting-state networks," *Front. Syst. Neurosci.*, vol. 5, p. 2, 2011.

[18] M. Termenon, A. Jaillard, C. Delon-Martin, and S. Achard, "Reliability of graph analysis of resting state fMRI using test-retest dataset from the human connectome project," *Neuroimage*, vol. 142, pp. 172–187, 2016.